Green Spectrofluorimetric Determination of Clemastine Using Nitrogen and Phosphorus Co-Doped Carbon Quantum Dots with Face-Centered Design Optimization and Sustainability Assessment

Ahmed A. Almrasy [a,*], Omkulthom Al kamaly [b], Mustafa Sayedahmed [c]

[a] Pharmaceutical Analytical Chemistry Department, Faculty of Pharmacy, Al-Azhar University, Nasr City 11751, Cairo, Egypt

[b] Department of Pharmaceutical Sciences, College of Pharmacy, Princess Nourah bint Abdulrahman University, P.O. Box 84428, Riyadh 11671, Saudi Arabia

[c] Analytical Research and Development Department, Benchmark Health Company, Cairo, Egypt

*Corresponding author email address (**Ahmed A. Almrasy**): ahmedalialmrasy8@gmail.com

Table S1: Face-centered central composite design matrix showing experimental runs with four factors at three levels each.

		Factor 1	**Factor 2**	**Factor 3**	**Factor 4**
Std	Run	A:pH	B:Buffer Volume	C:N,P CQDs	D:Time
			mL	µg/mL	min
19	1	6	0.25	120	9
13	2	3	0.25	200	15
7	3	3	1.5	200	3
12	4	9	1.5	40	15
15	5	3	1.5	200	15
10	6	9	0.25	40	15
2	7	9	0.25	40	3
9	8	3	0.25	40	15
1	9	3	0.25	40	3
17	10	3	0.875	120	9
8	11	9	1.5	200	3
25	12	6	0.875	120	9
3	13	3	1.5	40	3
27	14	6	0.875	120	9
4	15	9	1.5	40	3
6	16	9	0.25	200	3
22	17	6	0.875	200	9
11	18	3	1.5	40	15
21	19	6	0.875	40	9
26	20	6	0.875	120	9
23	21	6	0.875	120	3
20	22	6	1.5	120	9
24	23	6	0.875	120	15
16	24	9	1.5	200	15
5	25	3	0.25	200	3
14	26	9	0.25	200	15
18	27	9	0.875	120	9

Table S2: Model adequacy statistics for the reduced quadratic model.

Std. Dev.	**0.4379**	R^2	**0.9405**
Mean	4.09	**Adjusted R^2**	0.9186
C.V. %	10.71	**Predicted R^2**	0.8665
		Adeq Precision	21.5208

Table S3: Effect of common pharmaceutical excipients and endogenous biological components on clemastine determination.

Interfering Substance	**QE%**	**RSD%**	**Interference**
None (Clemastine alone)	81.32	1.52	-
Pharmaceutical Excipients			
Microcrystalline cellulose	82.18	1.58	No
Lactose monohydrate	80.14	1.88	No
Magnesium stearate	82.98	1.76	No
Polyethylene glycol	81.06	1.98	No
Hypromellose (HPMC)	81.52	2.03	No
Croscarmellose sodium	80.96	2.09	No
Colloidal silicon dioxide	82.16	1.7	No
Endogenous Biological Components			
Glucose	80.04	2.02	No
Urea	82.86	1.88	No
Uric acid	81.07	1.67	No
Creatinine	82.57	2.07	No
Albumin	83.9	1.46	No
Ascorbic acid	82.56	2.00	No
Cholesterol	80.71	2.14	No
Structural Analogs			
Diphenhydramine HCl	82.34	1.94	No
Chlorpheniramine maleate	81.89	2.08	No

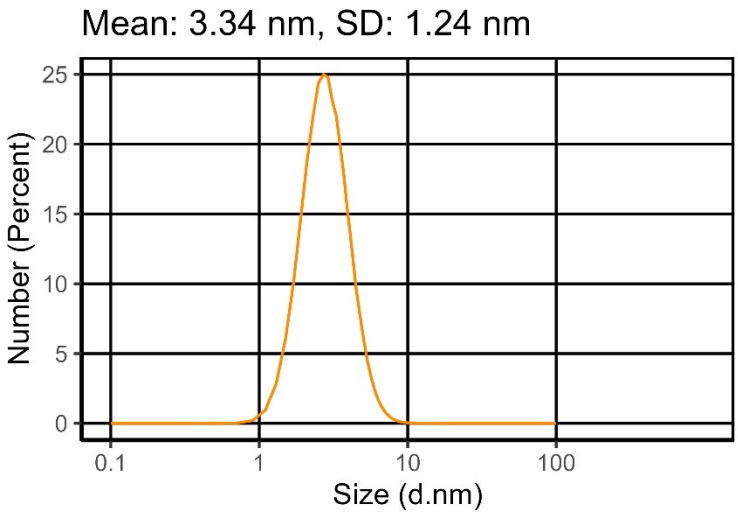

Fig. S1: Dynamic light scattering (DLS) size distribution analysis of N,P-CQDs in aqueous suspension showing hydrodynamic diameter and particle size distribution, confirming monodisperse nature in solution.

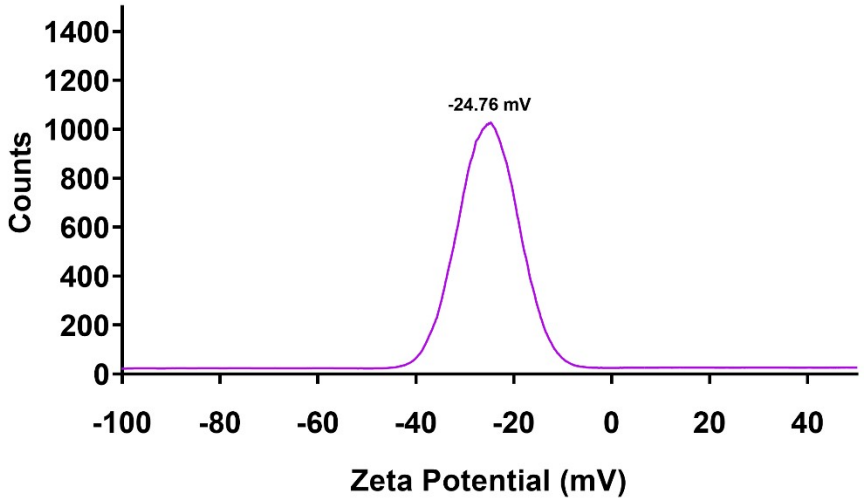

Fig. S2: Zeta potential distribution of N,P-CQDs in aqueous suspension measured by dynamic light scattering at 25°C, showing a zeta potential of −24.76 mV confirming the negatively charged surface and good colloidal stability of the synthesized nanoprobes.

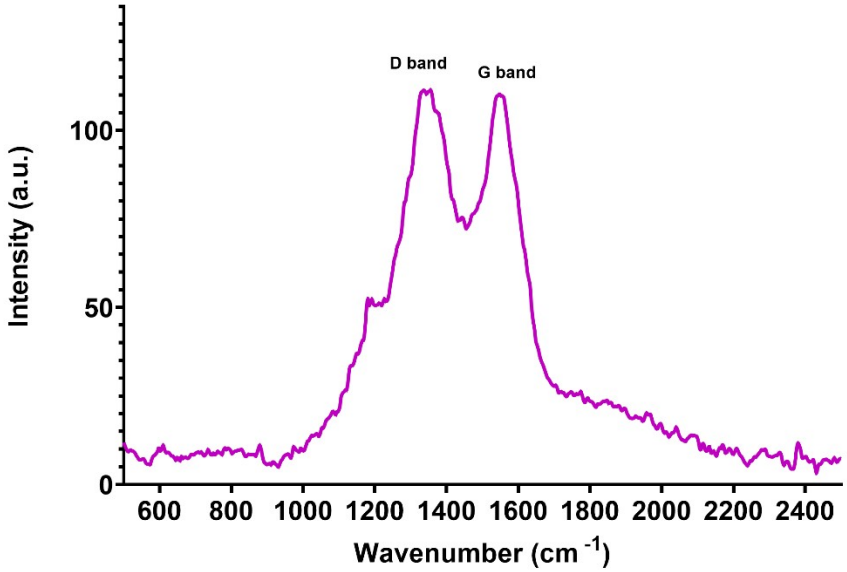

Fig. S3: Raman spectrum of the synthesized N,P-CQDs showing the characteristic D band at 1355 cm^{-1} and G band at 1548 cm^{-1} with an ID/IG ratio of 1.01, confirming successful heteroatom co-doping and defect-rich carbon nanostructure.

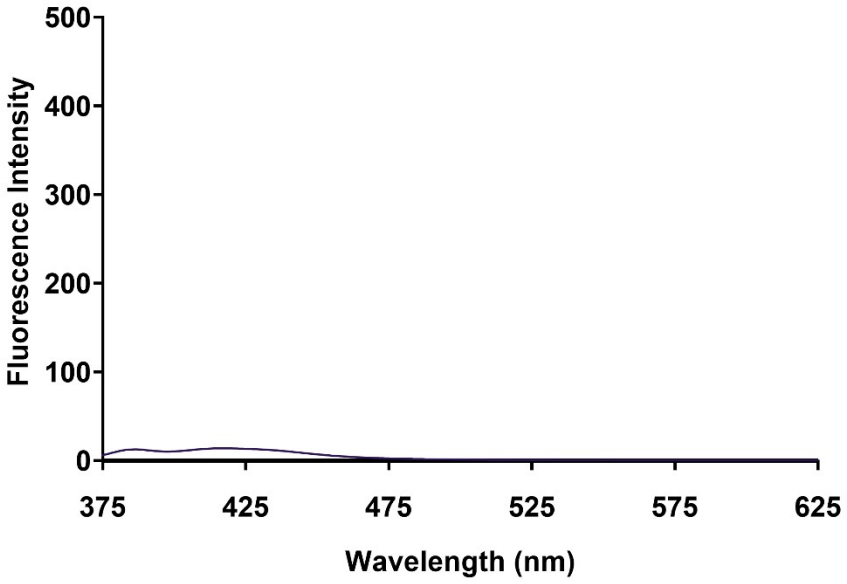

Fig. S4: Fluorescence emission spectrum of clemastine alone (4.0 µg/mL, excitation 345 nm) in the absence of N,P-CQDs, demonstrating negligible intrinsic fluorescence across the 375–625 nm emission range, confirming the absence of spectral interference from the analyte at the analytical working wavelengths.

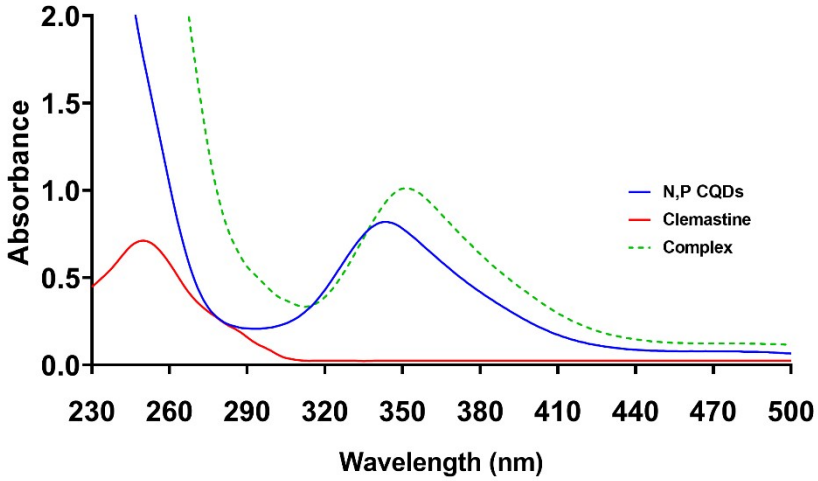

Fig. S5: UV-visible absorption spectra of N,P-CQDs alone (blue), clemastine alone (red), and the N,P-CQD-clemastine complex (green dashed), demonstrating hyperchromic effect and bathochromic shift of the N,P-CQD absorption peak upon complexation, confirming ground-state complex formation.

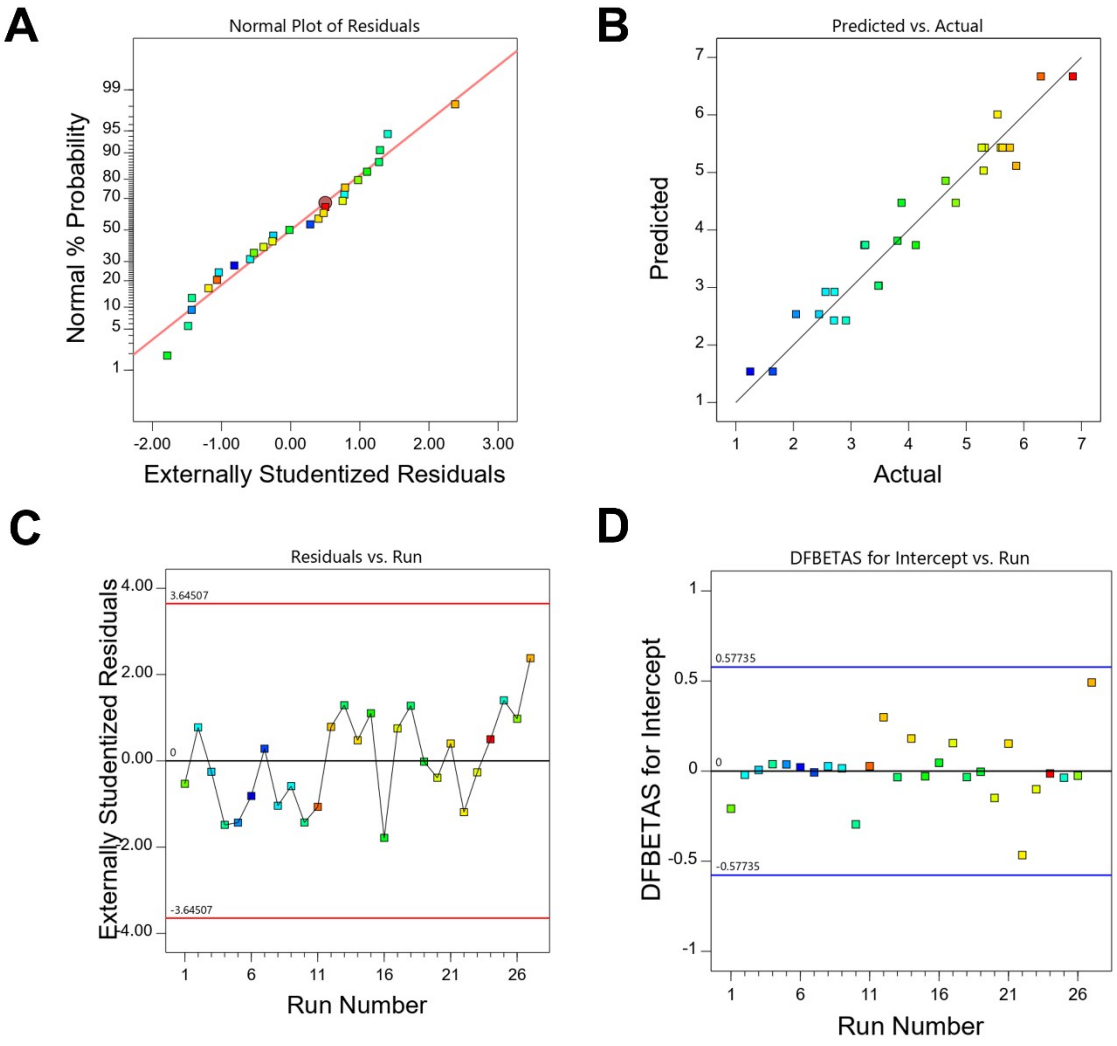

Fig. S6: Diagnostic plots for model validation of the reduced quadratic model from face-centered central composite design. (A) Normal probability plot of externally studentized residuals for error distribution assessment. (B) Predicted versus actual values plot for model prediction accuracy evaluation. (C) Residuals versus run number plot for systematic error detection. (D) DFBETAS plot for intercept showing absence of influential outliers.

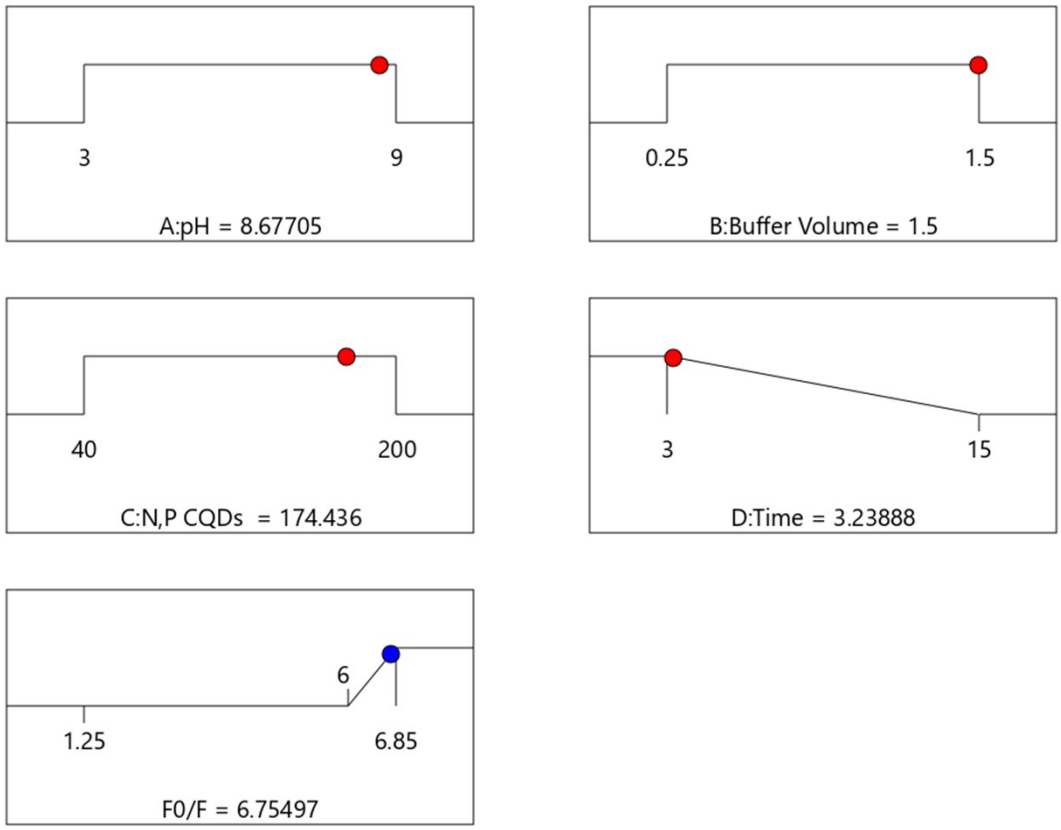

Fig. S7: Numerical optimization ramp displaying optimal factor settings determined by desirability function approach for maximizing fluorescence quenching efficiency (F0/F ratio). Optimal conditions include buffer pH, buffer volume, N,P-CQD concentration, and incubation time with corresponding predicted response value.

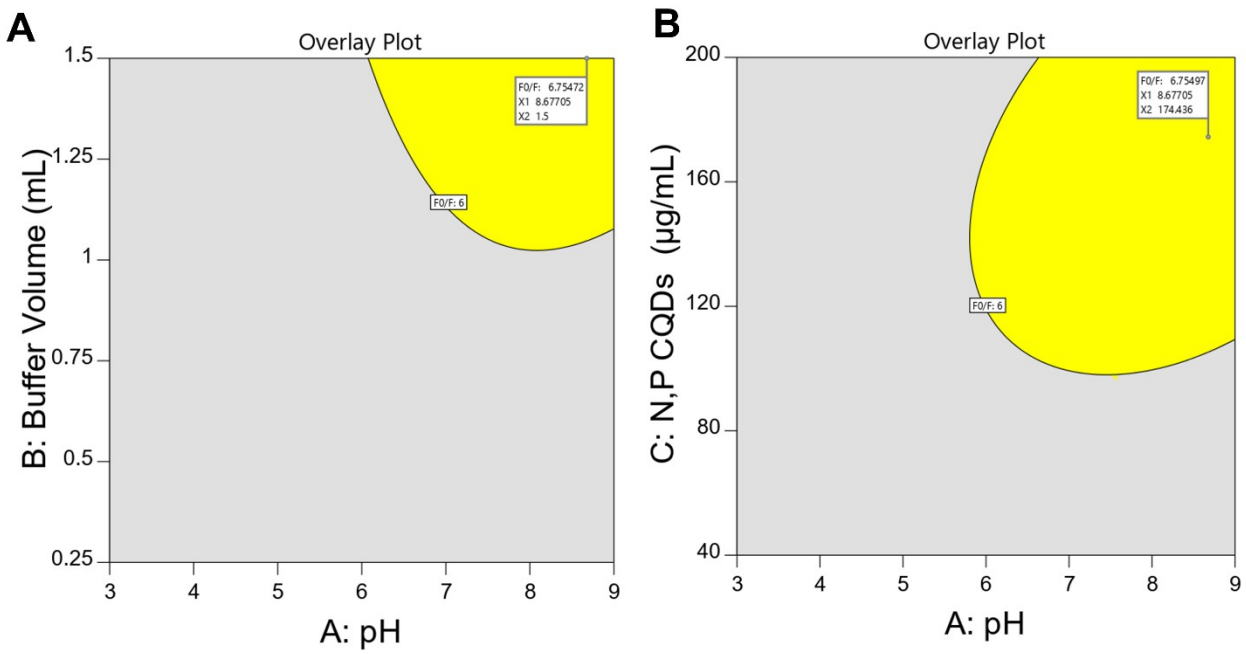

Fig. S8: Overlay plots showing design space regions (yellow-shaded areas) satisfying predetermined analytical performance criteria. (A) pH versus buffer volume design space. (B) pH versus N,P-CQD concentration design space. Feasible regions indicate method tolerance to minor variations in experimental conditions.